PERMEABILITY ESTIMATION USING PORE GEOMETRY ANALYSIS AND PERCOLATION THEORY IN CARBONATES

ESTIMATIVA DA PERMEABILIDADE USANDO ANÁLISE DA GEOMETRIA POROSA E TEORIA DE PERCOLAÇÃO EM CARBONATOS

PEDRO CANHAÇO DE ASSIS

UNIVERSIDADE ESTADUAL DO NORTE FLUMINENSE
LABORATÓRIO DE ENGENHARIA E EXPLORAÇÃO DE PETRÓLEO

MACAÉ - RJ
JULHO - 2019

PERMEABILITY ESTIMATION USING PORE GEOMETRY ANALYSIS AND PERCOLATION THEORY IN CARBONATES

ESTIMATIVA DA PERMEABILIDADE USANDO ANÁLISE DA GEOMETRIA POROSA E TEORIA DE PERCOLAÇÃO EM CARBONATOS

PEDRO CANHAÇO DE ASSIS

Dissertação apresentada ao Centro de Ciência e Tecnologia da Universidade Estadual do Norte Fluminense, como parte das exigências para obtenção do título de Mestre em Engenharia de Reservatório e de Exploração.

Orientador: Prof. Fernando Sergio de Moraes, Ph.D.

MACAÉ - RJ
JULHO - 2019

PERMEABILITY ESTIMATION USING PORE GEOMETRY ANALYSIS AND PERCOLATION THEORY IN CARBONATES

ESTIMATIVA DA PERMEABILIDADE USANDO ANÁLISE DA GEOMETRIA POROSA E TEORIA DE PERCOLAÇÃO EM CARBONATOS

PEDRO CANHAÇO DE ASSIS

Dissertação apresentada ao Centro de Ciência e Tecnologia da Universidade Estadual do Norte Fluminense, como parte das exigências para obtenção do título de Mestre em Engenharia de Reservatório e de Exploração.

Aprovada em 08 de julho de 2019.

Comissão Examinadora:

Irineu de Azevedo Lima Neto (D.Sc., Engenharia de Reservatório e de Exploração) - FACC

Marco Antônio Rodrigues de Ceia (D.Sc., Engenharia de Reservatório e de Exploração) - LENEP/CCT/UENF

Roseane Marchezi Misságia (D.Sc., Engenharia de Reservatório e de Exploração) - LENEP/CCT/UENF

Fernando Sergio de Moraes (Ph.D., Geofísica) - LENEP/CCT/UENF (Orientador)

This dissertation is dedicated to my parents Edmilson and Maria das Graças, my girlfriend Krystal, and extended family.

First and foremost, I would like to thank God for being my strength and guide during my life, and for giving me knowledge, ability and opportunity to complete this research study.

It is my great pleasure to thank committee members, family, friends and colleagues, whose support enables to me to complete this dissertation.

I would like to express my deepest gratitude to my Ph.D. advisor, Fernando Moraes, for his guidance and earnest help during the course of this project. I would like to thank my committee members, D.Sc. Irineu Lima, D.Sc. Marco Ceia and D.Sc. Roseane Misságia, for their supervision and profound advice in this research. This dissertation would not have been possible without their support throughout the whole process.

Thanks also to my parents Edmilson Moulins and Maria das Graças Canhaço, my sister Laryssa Canhaço, and my girlfriend Krystal Soares for their support and for giving me strength during this work.

I would also want to extend my appreciation to my friends and colleagues Igor Barbosa, Lucas Bomfim, Uilli Freitas, Maurício Matos, Renzo Francia, and the other members in the Reservoir Inference Group and Invision Geophysics, who were always willing to help and offer their best suggestion.

I would like to express my gratitude to the Reservoir Inference Group (GIR/LENEP/CCT/UENF) for providing great atmosphere and enough assistantship for this research.

Finally, I thank PETROBRAS for the financial support through a research grant (TC 0050.0079950.12.9) and the PFRH-PB 226 Graduate Program in Applied Geophysics. In addition, I express my gratitude to the Conselho Nacional de Desenvolvimento Científico e Tecnológico (CNPq) for the financial support of the INCT-GP and CAPES for the institutional and financial support.

Contents

List of Figures

List of Tables

Nomenclature

Latin Alphabet

a	Major semi-axis [m]
A	Area [m^2]
b	Minor semi-axis [m]
c	Pore connectivity
d	Curvature constant of connectivity function
D	Diameter [m]
e	Eccentricity
f	Pore space fraction
F	Formation factor
k	Permeability [mD]
K	Bulk modulus [GPa]
l	Pipe length [m]
L	Sample length [m]
m	Cementation coefficient
M	Number of inclusions
n	Number of pipes
N	Number of pore types
P	Geometrical factor of the inclusion models
q	Flow rate [m^3/s]
Q	Geometrical factor of the inclusion models
R	Radius [m]
R^2	Correlation coefficient
S	Specific surface [m^{-1}]
V	Volume [m^3]
Vp	Compressional velocity [m/s]
Vs	Shear velocity [m/s]

x	Volume fraction
z	Coordination number

Greek Alphabet

α	Aspect ratio
β	Function of the standard deviation of the pore radius distribution
γ	Gamma ray [API]
ΔP	Pressure drop [Pa]
Δt	Transit time [$\mu s/ft$]
η	Dynamic viscosity [cp]
μ	Shear modulus [GPa]
ρ	Density [Kg/m^3]
$\sum$	Summation
τ	Tortuosity
ϕ	Porosity
χ	Lime mud fraction

Subscripts

0	Solid component or mineral phase
1	Component or pore type 1
2	Component or pore type 2
$bulk$	Rock bulk
c	Critic threshold
$clean$	Absence of lime mud
d	Density
dry	Dry rock
$ellip$	Ellipsoid
est	Estimated
fl	Fluid
i	Index of the ith pore type
mlr	Multiple linear regression
mud	Lime mud

n	Neutron
o	Oil
$pore$	Porous space
s	Sonic
$sample$	Core sample
sat	Saturated rock
th	Percolation threshold
w	Water

Superscripts

$*$	Background medium
2	Component 2

Acronyms

DEM	Differential Effective Medium
FU	Flow Unit
KC	Kozeny-Carman
MLR	Multiple Linear Regression
NMR	Nuclear Magnetic Resonance

Abstract

This work present a new method for estimating permeability in carbonates from a set of conventional wireline logs, composed by gamma ray, neutron, density and sonic logs. The method is based on a modified Kozeny-Carman model, with derivation of pore geometry through the use of effective medium models and the concept of tortuosity. Percolation theory is then used to derive a pore connectivity coefficient which is calibrated according to the presence of carbonatic mud in the rock. The approach is evaluated by comparing permeability estimates with measured values of 173 core samples, from a carbonate oil field in Campos Basin, Brazil. This post-salt sequence comprises ramp deposits with various textures, including grainstones, packstones and mudstones, deposited in a marine environment of shallow platform. The results show that the proposed method can reproduce reasonably well permeability measurements over the range of 0.1 to 8100 mD in oil and oil-water transition zones comprising different carbonate textures, with porosity varying from 6 to 34%. The obtained correlation coefficient R^2 = 0.76 between measured and predicted permeability demonstrates the validity of the new approach and confirms that pore geometry and pore connectivity are the main parameters that control the fluid flow in porous media. These parameters can then be used in specialized models to reduce the permeability estimation errors.

Keywords: carbonates, permeability, percolation, pore connectivity, pore geometry.

Resumo

Este trabalho apresenta uma nova metodologia para estimar a permeabilidade em carbonatos a partir de um conjunto de perfis convencionais de poço formado por raios gama, neutrônico, densidade e sônico. O método é baseado em uma modificação do modelo de Kozeny-Carman, onde a estimativa da geometria porosa é realizada através do uso de modelos de meio efetivo e do conceito de tortuosidade. A teoria da percolação é então usada para modelar um coeficiente de conectividade dos poros, o qual é calibrado de acordo com a presença de lama carbonática na rocha. A metodologia é avaliada comparando-se as estimativas de permeabilidade com os valores medidos de 173 amostras de laboratório pertencentes a um campo de óleo carbonático na Bacia de Campos, Brasil. Essa sequência do pós-sal compreende depósitos em rampa com várias texturas, incluindo grainstones, packstones e mudstones, depositados em um ambiente marinho de plataforma rasa. Os resultados demostram que o método proposto é capaz de reproduzir razoavelmente bem as medidas de permeabilidade na faixa de 0,1 a 8100 mD em zonas de óleo e transição óleo-água, compreendendo diferentes texturas carbonáticas e com porosidade variando entre 6 e 34%. O coeficiente de correlação R^2 = 0,76 obtido entre a permeabilidade medida e estimada reitera a validade do modelo e demostra que a geometria porosa e a conectividade dos poros são os principais parâmetros que controlam o fluxo de fluidos em meios porosos. Esses parâmetros podem então ser utilizados em modelos especializados para reduzir os erros de estimativa da permeabilidade.

Palavras chave: carbonatos, permeabilidade, percolação, conectividade dos poros, geometria porosa.

1 Introduction

The reservoir management requires a deep knowledge of the reservoir that can be achieved only through its characterization by a process of acquiring, processing and integrating several basic data. Throughout this dynamic process, the permeability plays a central role since it measures the capacity and ability of the formation to transmit fluids. Even when considering a single rock type, it can vary over several orders of magnitude, depending on parameters related to the rock framework, such as porosity, pore size and pore connectivity. For that reason, the permeability can be considered one of the most elusive parameter estimation problem during the reservoir characterization. In relation to carbonate rocks, which represent more than 60% of the world's oil reserves, the permeability estimation becomes an even greater challenge due to the associated heterogeneity, related to diagenetic processes, architecture and structural complexity.

Permeability can be measured from laboratory using core samples or at the wells using formation testers at selected depth points. Since both techniques are expensive, time-consuming and sparse, several models and empirical relationships have been developed in an attempt to reproduce permeability measurements from wireline logs. Some of these methods usually express the permeability as function of physical properties of the pore system, such as porosity. Although it is a common sense to assume that permeability depends on porosity, it is well-know that two porous systems can have similar porosities but different permeabilities. This lack of correspondence can be attributed to differences in the initial grain size, sorting and diagenetic history, which indicate that only single relations between permeability and porosity are not able to provide reliable permeability estimations (NELSON, 1994).

There are other methods that relate the permeability with different rock properties such as resistivity and water saturation, e.g., Timur (1968), Coates and Dumanoir (1973), Katz and Thompson (1986), and de Lima (1995). Although these models can also estimate permeability from wireline logs, they usually have constants and parameters that require core samples for calibration, and therefore, have their applicability

restricted to a specific field. More reliable methods for indirect prediction of permeability are those based on the Nuclear Magnetic Resonance (NMR) and Stoneley wave logging, which, however, are more often not available. Other methods for permeability estimation also involve Multiple Linear Regression (MLR) and Neural Networks (HUANG *et al.*, 1996), however, such methodologies lack physical-theoretical justification and require large core datasets for model calibration, which difficult the general application of the method.

Many researchers have attempted estimate permeability based on rock framework analysis, since the flow capacity is directly correlated with the pore geometry and connectivity (LØNØY, 2006). In this context, several relations derived from Kozeny-Carman (CARMAN, 1961) have been proposed in order to improve the permeability estimation, since the Kozeny-Carman (KC) model considers geometrical properties of the porous space, like, specific surface, tortuosity and, in some modifications, the percolation behavior. Prasad (2003), for example, analyzed the influence of pore geometry on the relation between permeability, velocity and porosity through flow unit concept, and Mavko and Nur (1997) modified the KC model inserting a percolation threshold on porosity, which improved the permeability estimation in clean, well-sorted rocks.

Considering that both permeability and velocities are affected by pore geometry and pore connectivity, Eberli *et al.* (2003) investigated the relationship between them in carbonate rocks, and stated that permeability and velocities are more affected by these properties than by the total porosity of the rock. Fabricius *et al.* (2007) have also developed relations between pore geometry and ultrasonic velocities from laboratory core data to estimate permeability, and in a more recent approach, Saxena (2017) correlated permeability with elastic properties through the characterization of pore geometry using an effective percolated medium model and a connectivity function based on percolation theory.

Bernabé *et al.* (2010) also derived a permeability model based on pore networks simulations considering the Poiseulle and Darcy's laws (the same assumption of the KC model) parameterized in terms of pore size and connectivity, expressed respectively as pore radius and pore coordination number. In their model, the relation between permeability k and coordination number z follows a power law relation, in the sense of percolation theory, expressed by $k \propto (z - z_c)^{\beta}$, where the exponent β is a function of the standard deviation of the pore radius distribution and z_c is the percolation threshold expressed in terms of the coordination number. To enhance the applicability of the model, Bernabé *et al.* (2011) replaced the coordination number by introducing the

resistivity formation factor F, since they found that k and F obey "universal" power laws of $(z - z_c)$. They satisfactorily tested the model by comparison with published experimental data on a variety of granular materials and rocks.

Thus, considering the effect of pore heterogeneity and pore connectivity on permeability, the development of a physical-theoretical model that integrates conventional geophysical logs, so that effectively describes the pore geometry without becoming too complex (so that it becomes impractical), would have wide applicability, since it would allow continuous permeability curves along the well, reducing the dependence on special logs and large core sample datasets. Therefore, considering that there is currently no general model capable of estimating permeability from conventional wireline logs with a reasonable degree of uncertainty, this work present a new method to improve the permeability prediction in carbonate rocks using a modified Kozeny-Carman model, which takes into account the modeling of pore geometry through the use of effective medium models and the concept of tortuosity, and the percolation theory to model the pore connectivity.

2 Method

Considering the problem of estimating absolute permeability from a set of conventional wireline logs, this section present a modified form of the Kozeny-Carman model, which takes into account the effect of pore geometry and pore connectivity. It is also presented a brief review of the main concepts and models used during the estimation of permeability model parameters, which involve the use of effective medium models, the concept of tortuosity and percolation theory.

2.1 The Permeability Model

The proposed permeability model is built on top of Kozeny-Carman model, which is originally derived from the Poiseulle and Darcy's laws (see Appendix A), by introducing a percolation term c that models the connectivity of the porous space to obtain the permeability k, as given by

$$k = \frac{c}{2}\frac{\phi^3}{S^2\tau^2}, \tag{2.1}$$

where the permeability is expressed in units of m^2, c represents the pore connectivity, ϕ the porosity, S the specific surface, defined as the ratio of porous surface area to rock bulk volume, expressed in units of m^{-1}, and τ the tortuosity, that represents the ratio of total flow-path length to length of the sample.

About these model parameters, the porosity ϕ, which represents the storage capacity of the rock, can be derived from density, sonic and neutron logs by well-known methods. Considering the porosity from density logs ϕ_d, the most common approach is the well-know mass balance equation

$$\phi_d = \frac{\rho_0 - \rho}{\rho_0 - \rho_{fl}}, \tag{2.2}$$

where ρ, ρ_0 and ρ_{fl} represent the densities of the log reading, of the solid rock component, and of the pore fluid, respectively.

The porosity from sonic logs ϕ_s can be derived from Wyllie Time Average equation (WYLLIE *et al.*, 1956), given by

$$\phi_s = \frac{\Delta t - \Delta t_0}{\Delta t_{fl} - \Delta t_0}, \tag{2.3}$$

where Δt, Δt_0 and Δt_{fl} are the transit times of the log reading, of the solid rock component, and of the pore fluid, respectively.

The neutron porosity ϕ_n is measured directly from neutron log, and the porosity prediction can be improved from a combination of these three log porosities using the conventional Multiple Linear Regression (MLR) approach.

The other model parameters connectivity c, specific surface S, and tortuosity τ have their estimation procedures described in the next sections.

2.2 Pore Connectivity

Since the real pore geometry is not consistent with the pipe-like geometry of the original KC model, which often provides overestimated permeability values when compared with the measured ones, the original model is modified by introducing a percolation term c that models the connectivity of the porous space, based on percolation theory, to obtain the more reliable permeability estimations.

The percolation theory has been a promising approach to quantify interconnectivity effects of a system on its flow and transport properties through universal laws, where the degree of connection accounts for the fraction of pores that belong to an infinite network (BERNABÉ *et al.*, 2010; GHANBARIAN *et al.*, 2013).

This behavior is inserted in the permeability model by considering the rock as a mixture of granular and matrix components, having matrix volume fraction χ, here representing lime mud, which can be estimated from gamma ray logs γ considering the cutoffs of the zones without the presence of lime mud γ_{clean} and completely formed by carbonate mud γ_{mud} (e.g., mudstones):

$$\chi = \frac{\gamma - \gamma_{clean}}{\gamma_{mud} - \gamma_{clean}}. \tag{2.4}$$

Since the universal features of percolation theory determine the form of the connectivity function, the pore connectivity c can be parameterized in terms of χ assuming that the amount of mud controls the flow capacity of the rock, specially depending how it is distributed in the rock frame, which can reduce the pore throat size and consequently the connectivity of the pores.

Thus, the connectivity function c can be modeled by a percolation behavior, as given by

$$c(\chi) = \left[1 - \left(\frac{\chi - \chi_{th}}{\chi_c - \chi_{th}}\right)^d\right], \tag{2.5}$$

where the subscripts th and c represent the values of χ which the connectivity starts to be different from 1 and becomes zero, respectively. The constant d is the factor responsible for controlling the curvature of the function.

The Fig. 1 shows the behavior of c as a function of the lime mud volume χ considering several values for the curvature constant d. For this case, the cutoffs χ_{th} and χ_c were defined with 0 and 0.7, respectively. As can be observed in Fig. 1, in the transition phase, the increment in the lime mud volume causes a reduction in the pore connectivity, and its intensity is directly related to the constant of curvature d.

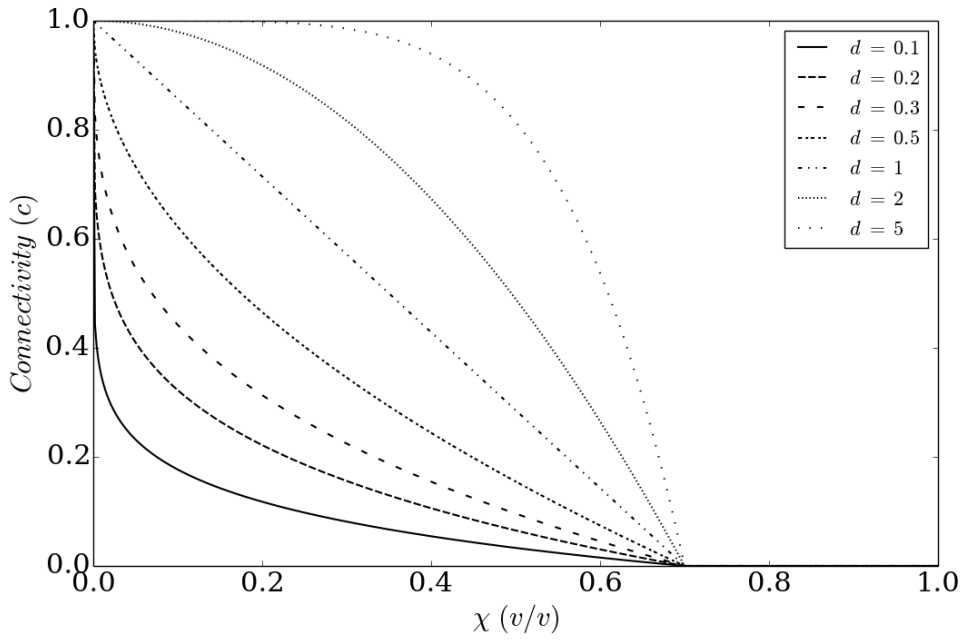

Figure 1: The connectivity function c as a function of the lime mud volume χ, for several curvature values d. The cutoffs χ_{th} and χ_c were defined with 0 and 0.7, respectively.

This percolation behavior tends to improve the permeability estimation in more heterogeneous granular rocks, since the original KC model does not take into account the interconnectivity of the pores.

2.3 Specific Surface Estimation

The specific surface S, defined as the ratio of porous surface area to rock bulk volume, have been estimated in laboratory from methods based on nitrogen adsorption and digital image analysis, or in wells from correlations with the relaxation times obtained from NMR logs (HEARST; NELSON, 1985).

In this work, a new approach for S is proposed using the Differential Effective Medium (DEM) model (BERRYMAN, 1992; MAVKO *et al.*, 2009), which estimates changes on the composite elastic moduli due to the presence of isolated ellipsoidal inclusions in a host medium, being able to define the pore geometry of the rock through concentration and shape of the pores (see Appendix B).

The model considers the pores like ellipsoidal inclusions with semi-axes a and b (Fig. 2), aspect ratio α and eccentricity e, respectively given by b/a and $\sqrt{1-\alpha^2}$, and surface area A_{ellip} and volume V_{ellip} defined by

$$A_{ellip} = 2\pi a^2 \left(1 + \frac{1-e^2}{e} arctanh(e)\right), \tag{2.6}$$

$$V_{ellip} = \frac{4\pi}{3} a^3 \alpha. \tag{2.7}$$

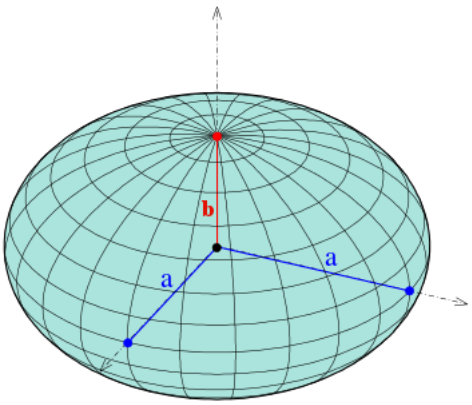

Figure 2: Ellipsoidal inclusion of semi-axes a and b.

Considering a porous space composed by N pore types, where for each pore type the inclusions have the same shape and size, it is possible to calculate the specific

surface S through the equation

$$S = \sum_{i=1}^{N} x_i \frac{A_{ellip\,i}}{V_{ellip\,i}}, \tag{2.8}$$

where x_i is the volume fraction for each pore type (see Appendix C for the complete equation derivation).

As can be observed from Eq. 2.6, 2.7 and 2.8, the specific surface S depends only on the concentration x (volumetric parameter), the aspect ratio α (pore shape) and the major semi-axis a (pore size) of the N inclusion types. In this work, these parameter estimations followed a methodology similar to Xu and Payne (2009), where the total porosity ϕ of the rock is divided into two dominant pore types, which each pore type should have its own fraction, shape and size.

In relation to the pore aspect ratio α and pore size a, their estimative can be realized from digital image analysis from thin sections or considering reference values for each pore type when the texture information is available, e.g., Xu and Payne (2009) and Lima Neto (2015) for pore shape, and Choquette and Pray (1970) for pore size. The estimation of each pore type fraction is then performed using the DEM inclusion model by modeling the relation between the compressional velocity Vp and the porosity ϕ for different fractions of each pore type (Fig. 3).

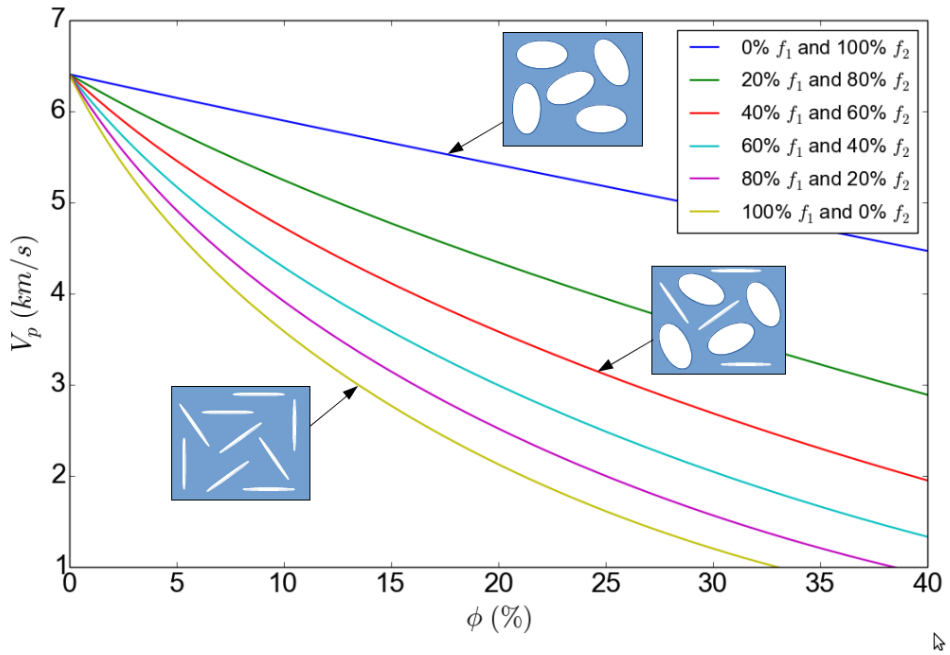

Figure 3: DEM rock physics template for Vp and porosity ϕ. The curves represent different pore fractions f_1 and f_2 for a dual porosity model with dry inclusion aspect ratios of α_1 = 0.05 and α_2 = 0.55 in a calcitic host medium.

Fixing the aspect ratio α for each pore type, the pore type fractions f are estimated from the analysis of which fractions, when composing the total porosity of the rock, estimate the DEM modeled compressional velocity Vp with the smallest error when compared real Vp measured by the logging tool. During this step, dry ellipsoidal inclusions are initially considered in a host medium formed by the mineral calcite and being subsequently saturated with the Gassmann (1951) equations (described in Appendix D).

Therefore, from the predefined size and shape of the inclusions for each pore type and considering their estimated fractions from the DEM model, it is possible to estimate the specific surface through the Eq. 2.8.

2.4 Tortuosity Estimation

The tortuosity τ, defined as the ratio of total flow-path length to length of the sample, is an important geometric parameter for permeability estimation through the Kozeny-Carman model, however, due to its high degree of uncertainty, many researchers ignore its physical meaning considering it as a calibration parameter of the model.

Some works have presented correlations between tortuosity and the formation factor F, defined as the ratio of the resistivity of a fluid filled rock to the resistivity of that fluid. Wyllie and Rose (1950), for example, considering that the resistivity of a porous medium is proportional to the porosity, stated that F increases with the decrease of porosity ϕ through a factor defined as tortuosity:

$$F = \frac{\tau}{\phi}. \tag{2.9}$$

Archie (1942) derived an empirical relationship, in which F varies with ϕ for a group of rocks with uniform lithology through the equation

$$F = \phi^{-m}, \tag{2.10}$$

where the parameter m is the cementation coefficient, which can vary from 1.3 to 3, and for intergranular rocks is approximately 2 (ARCHIE, 1942; WYLLIE; ROSE, 1950).

Substituting the Eq. 2.10 in Eq. 2.9, the tortuosity τ can be estimated from porosity

ϕ and cementation coefficient m, as given by

$$\tau = \phi^{1-m}, \tag{2.11}$$

where the rock becomes more tortuous with the reduction of porosity and with the increase of the cementation coefficient m.

3 Sensitivity Analysis of the Permeability Model

The sensitivity analysis of the modified Kozeny-Carman model aims to identify the influence of model parameters on the relation between permeability k and porosity ϕ. The initial model parameters consider an idealized dual porosity rock framework, where the features for the pore type 1 are associated to microcracks, having aspect ratio α_1 = 0.05, major semi-axis a_1 = 0.03 mm and pore fraction f_1 = 40%, and for the pore type 2 are associated to interparticle pores, with aspect ratio α_2 = 0.55, major semi-axis a_2 = 0.5 mm and pore fraction f_2 = 60%. The pore connectivity c and the tortuosity τ are initially defined as 0.7 and 2, respectively.

Considering the well-known scatter in the relation between k versus ϕ, the Fig. 4 analyzes the influence of tortuosity τ, which significantly reduces k for the entire range of ϕ. In relation to the pore connectivity c, the Fig. 5 shows that c increases k at a given ϕ, resulting in a vertical linear displacement of the curve k versus ϕ.

With respect to the variation of pore aspect ratio α, the pore type 1 presents a large variation of k for a given ϕ (Fig. 6), whereas the pore type 2 is almost non-sensitive with these changes (Fig. 7). This behavior can be explained since the roundness of the pores improves the aperture to fluid flow, and this effect has more influence on small pores present in the rock.

About the pore size a, the pore type 1 (Fig. 8), with low aspect ratio, presents more variation of k at a given ϕ than pore type 2 (Fig. 9). Considering the initial conditions of pore type 2, the improvement in k with the variation of a_1 occurs mainly because both pore types have better fluid flow conditions. However, varying a_2 the same improvement in k is not perceived, since the initial geometry of the pore type 1 does not contribute to fluid flow.

The Fig. 10 analyzes the variation of pore fractions f_1 and f_2, where the increasing of f_1 significantly reduces k for a certain ϕ, principally for low fractions (f_1 < 20%). This

fact confirms the premise that the presence of pores with small size and aperture in the pore space tends to reduce the permeability in rocks.

This sensitivity analysis showed that permeability is strongly dependent on tortuosity, pore connectivity and pore geometry, which the last one can be parameterized in terms of size, shape and fraction of the pore types. Thus, the proposed dual porosity model can be applied for permeability prediction in more heterogeneous rocks, such as carbonates.

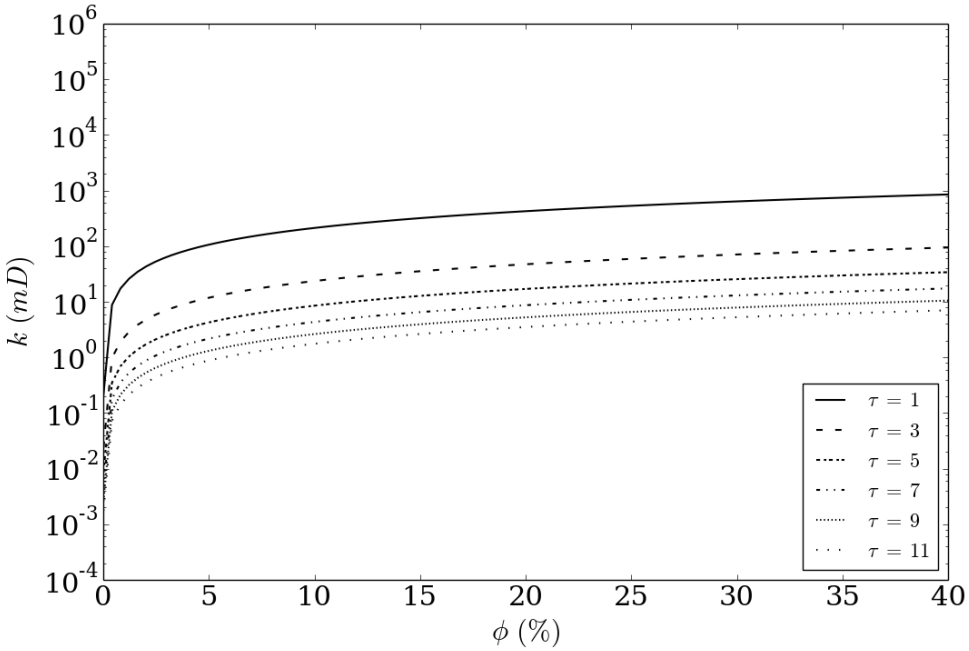

Figure 4: The KC model curves of permeability k versus porosity ϕ, considering the variation of tortuosity τ for a dual porosity rock framework.

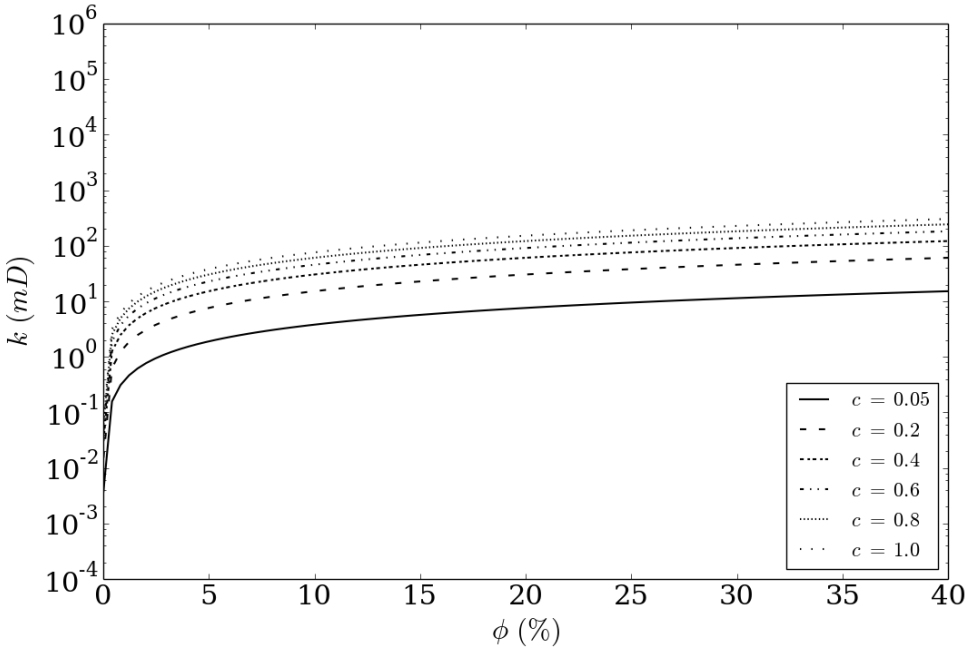

Figure 5: The KC model curves of permeability k versus porosity ϕ, considering the variation of pore connectivity c for a dual porosity rock framework.

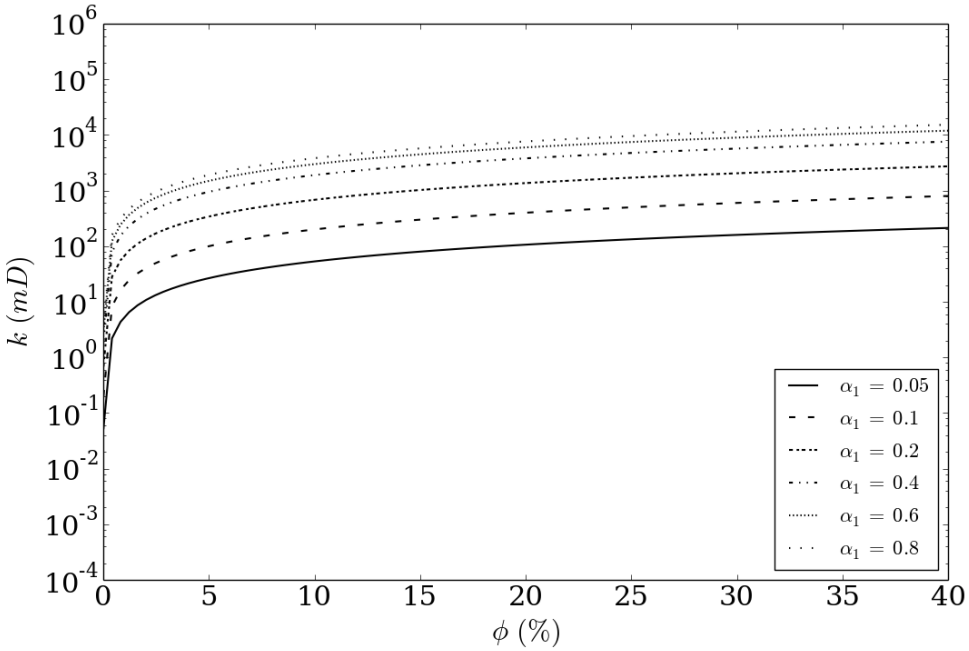

Figure 6: The KC model curves of permeability k versus porosity ϕ, considering the variation of aspect ratio α_1 for a dual porosity rock framework.

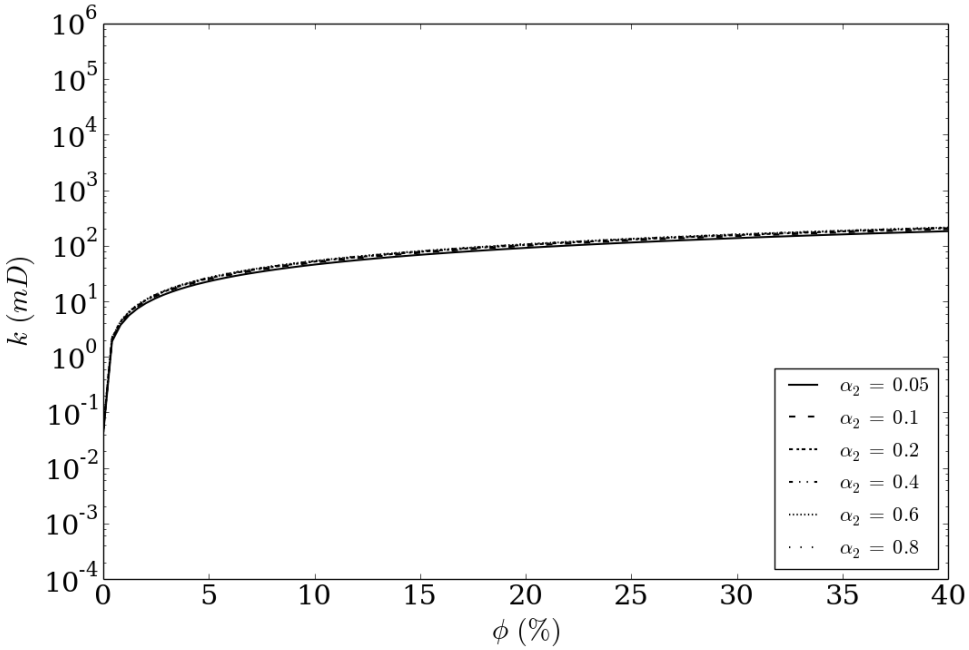

Figure 7: The KC model curves of permeability k versus porosity ϕ, considering the variation of aspect ratio α_2 for a dual porosity rock framework.

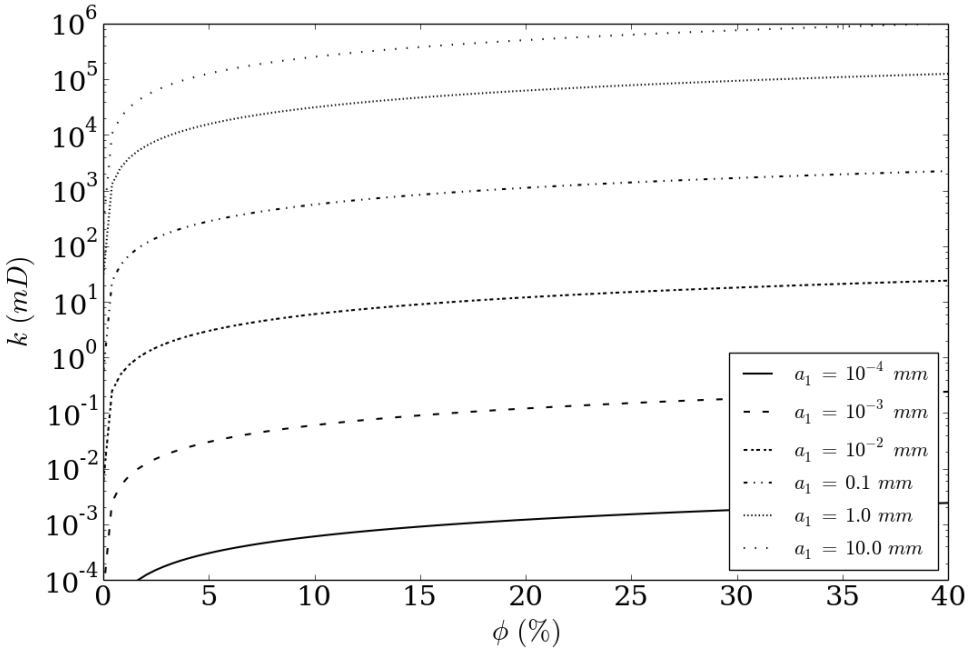

Figure 8: The KC model curves of permeability k versus porosity ϕ, considering the variation pore size a_1 for a dual porosity rock framework.

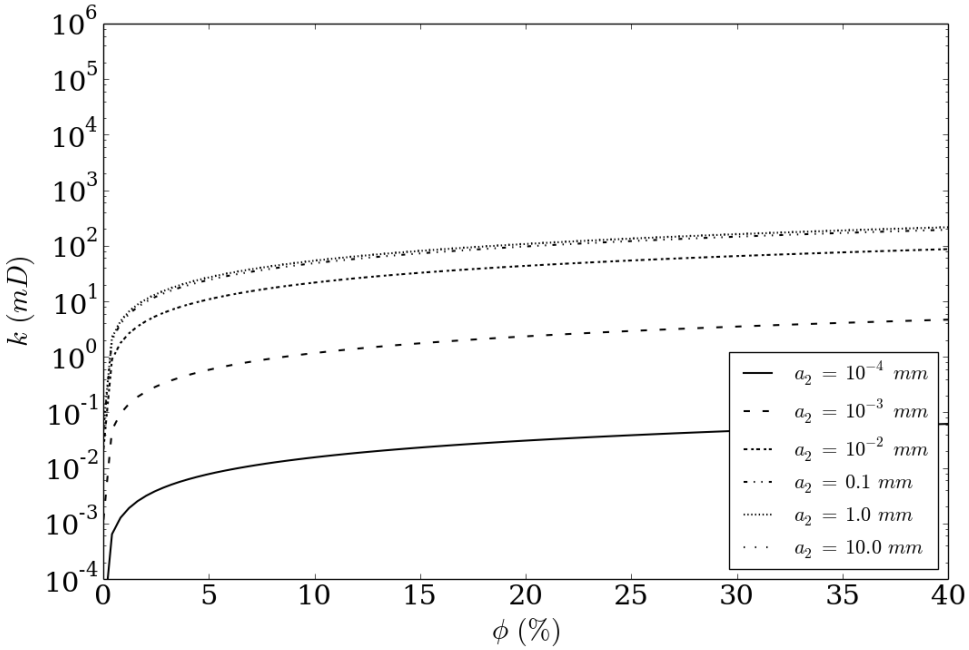

Figure 9: The KC model curves of permeability k versus porosity ϕ, considering the variation of pore size a_2 for a dual porosity rock framework.

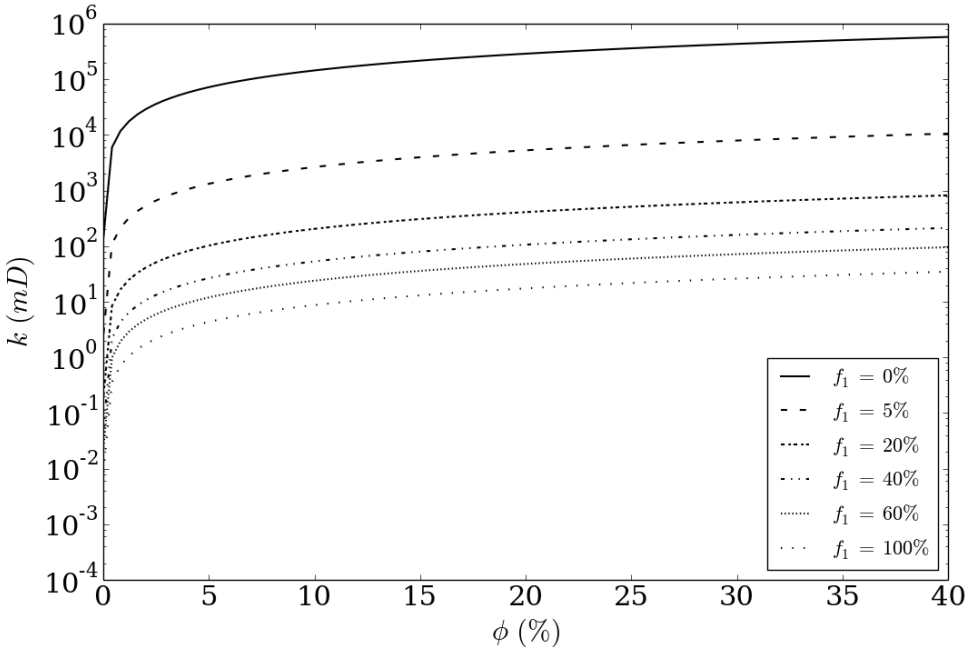

Figure 10: The KC model curves of permeability k versus porosity ϕ, considering the variation of pore fraction f_1 for a dual porosity rock framework.

4 Field Data Application

The new method is applied in a dataset from an Albian carbonate sequence deposited in a marine environment of shallow platform, in Campos Basin, which is located along the continental shelf of Rio de Janeiro State, southeastern Brazil. The basin covers an area of approximately 100.000 km^2 and corresponds to the main sedimentary area already explored off the Brazilian coast, comprising currently 41% of the country's oil production (Carrasquilla and Nelson, 2014).

The post-salt carbonate sequence comprises ramp deposits with various textures, such as grainstones, packstones, wackestones and mudstones, stacked on sea level change cycles related to high, moderate and low energy of the depositional environment. During higher sea levels, mudstones and wackestones with carbonatic mud associated are found. Given the complex heterogeneity of carbonate reservoirs, normally it exists a low recovery factor, and a difficult correlation between rock properties and geophysical data.

From the 27 drilled wells in the field, the selected well A10 has a more complete dataset, including basic geophysical logs (gamma ray, resistivity, density, neutron, and sonic), laboratory petrophysical data (porosity and permeability) and geological interpretation (lithofacies and stratigraphy). The depth interval studied in this work varies from 1758 to 1841 m and comprises an oil and oil-water transition zones with different carbonate textures.

Aiming to identify and characterize the oil reservoir and the oil-water contact, the Fig. 11 shows a basic log plot containing depth (1), facies texture description from core and thin section analysis considering the Dunham (1962) classification (2), gamma ray and compressional slowness (3), deep and shallow electrical resistivity (4), bulk density and neutron porosity (5), and water saturation (6).

The facies description and gamma ray log are good indicators of sea level changes during the deposition of the sediments that constitute the formations. The top of the reservoir, identified close to 1758 m, is characterized by a significantly decreasing in

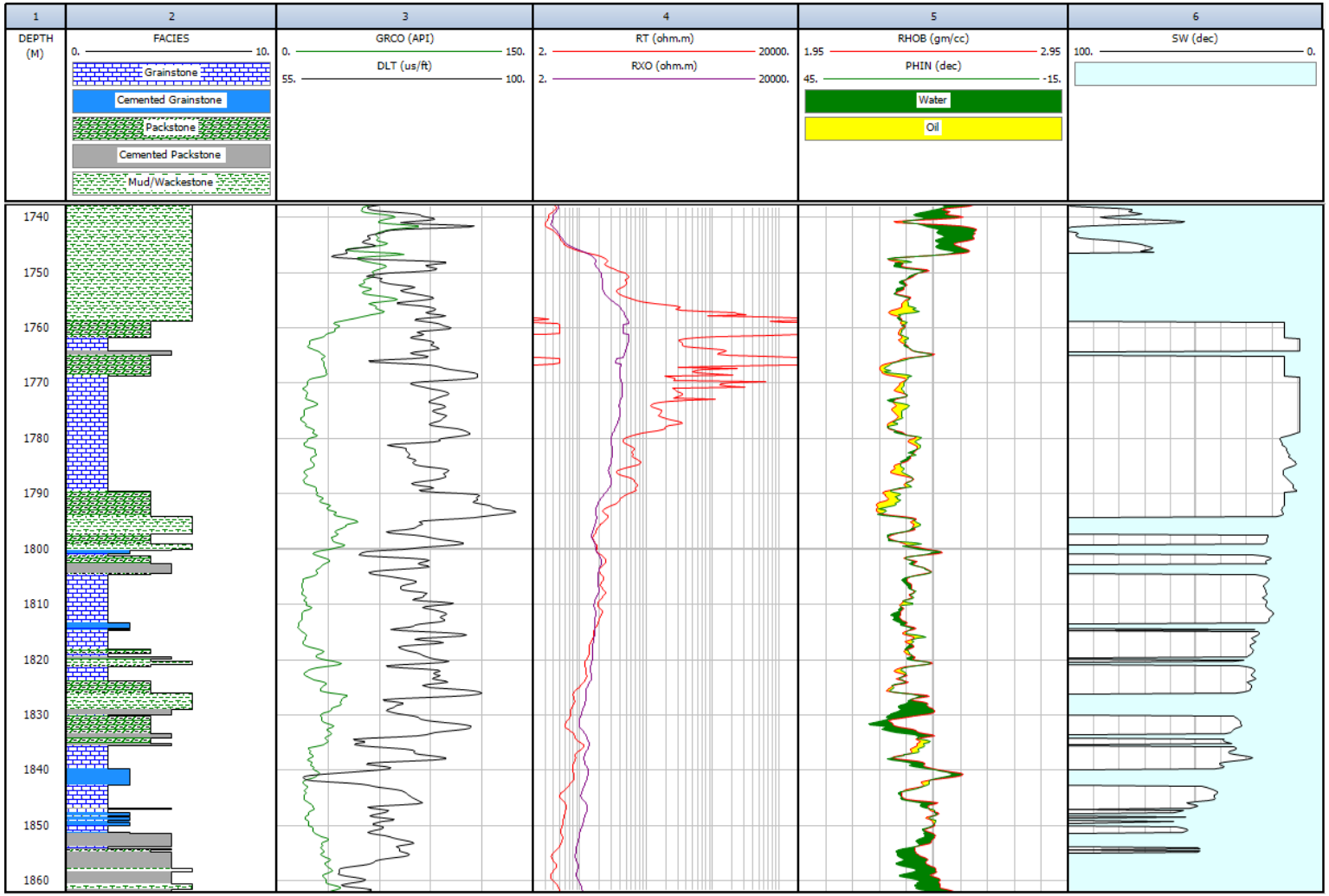

Figure 11: Basic log plot showing from the left to the right: 1 - depth, 2 - textural description, 3 - gamma ray and compressional slowness, 4 - deep and shallow electrical resistivity, 5 - bulk density and neutron porosity, 6 - water saturation.

the gamma ray log and for an increasing in the deep resistivity. The oil interval is also characterized by a crossover between bulk density and neutron logs represented by the yellow color. The oil-water contact is close to 1820 m, once the drilling mud is water based and the deep resistivity decreases approaching the invaded zone resistivity. The sonic log ranges from 60 to 100 us/ft and this variation is associated to the reservoir heterogeneity involving different pore types, the presence of lime mud and the occurrence of cementation in some intervals.

Considering the laboratory data, 173 core samples covering the oil and oil-water transition zones were selected. This dataset presents high porosity values varying from 6 to 34% and a wide permeability range from 0.1 to 8100 mD. Initially, the relation between permeability and porosity was investigated (Fig. 12), and as it can be seen, the permeability shows a considerable scatter at a given porosity indicating lack of correspondence between these two properties. This spreading indicates that factors like pore geometry and pore connectivity can have more influence on permeability than porosity, requiring more specialized models to improve the prediction of permeability.

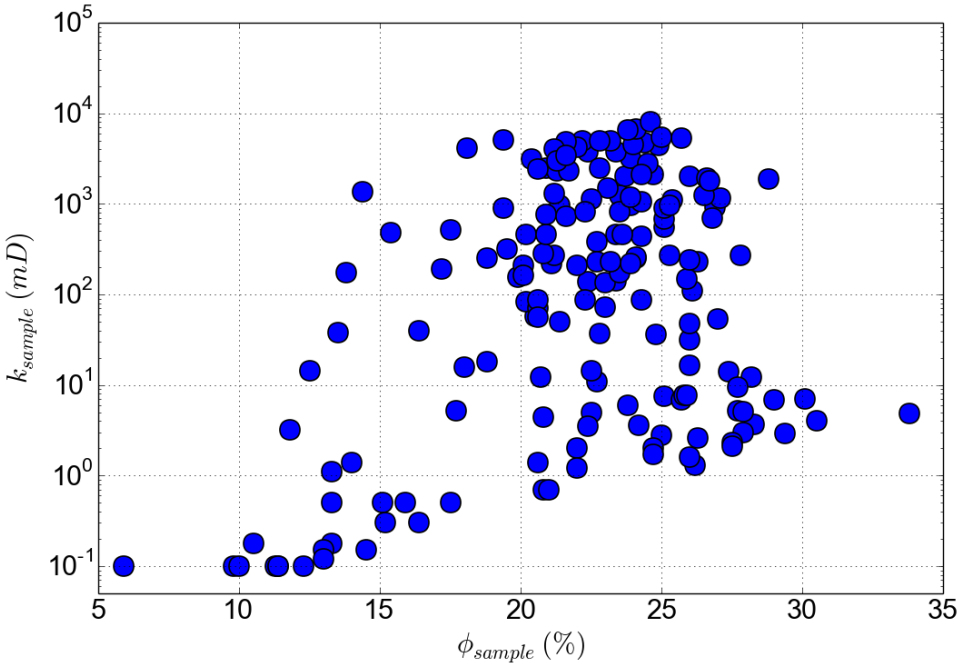

Figure 12: Crossplot of permeability k_{sample} and porosity ϕ_{sample} from laboratory core data, indicating lack of correspondence between these properties.

The porosity is estimated from well logs neutron, density and sonic, comparing the results with laboratory measurements. The neutron porosity ϕ_n is measured directly from the neutron log, while the density porosity ϕ_d and the sonic porosity ϕ_s are estimated through the mass balance equation (Eq. 2.2) and the Wyllie Time Average

equation (Eq. 2.3), respectively.

The input parameters of Eq. 2.2 and 2.3 consider the density and the slowness of mineral calcite, respectively given by ρ_0 = 2.71 g/cm^3 and Δt_0 = 46.7 us/ft (MAVKO *et al.*, 2009). The parameters for the pore fluids are estimated from Batzle and Wang (1992) equations considering the water saturation in the pore space. Since the initial pressure of the reservoir is 18.34 MPa, the average temperature is 70°C, the water salinity is 90000 ppm, and the oil density, in standard conditions, is 21 API, the fluid properties estimated from Batzle and Wang's equations are ρ_w = 1.06 g/cm^3 and Δt_w = 183.4 us/ft for water, and ρ_o = 0.89 g/cm^3 and Δt_o = 220.9 us/ft for oil.

The measured porosity from neutron log and the estimated porosities from density and sonic logs are shown in Fig. 13, in tracks 1, 2 and 3, respectively. The core sample porosity is also shown in Fig. 13 and exhibits low correlation with the log estimative, having correlation coefficient R^2 equals to 0.30, 0.32 and 0.06 for neutron, density and sonic porosities, respectively. The correlation coefficient between log and laboratory porosity is improved by performing a Multiple Linear Regression (MLR), which combines the neutron ϕ_n, density ϕ_d and sonic ϕ_s fractional porosities, as given by

$$\phi_{mlr} = 0.19\phi_n + 0.97\phi_d - 0.02\phi_s - 0.01. \tag{4.1}$$

The MLR porosity ϕ_{mlr}, shown in Fig. 13-4, improves the porosity prediction, increasing the correlation coefficient R^2 to 0.44. It is expected that small differences between measured and predicted porosity do not contribute to high errors on permeability estimative, since according to KC model, small variations on porosity do not contribute for high variations on permeability, principally for higher porosities.

The specific surface S is predicted from Eq. 2.8 by modeling a rock with two pore types, having respectively aspect ratios α_1 and α_2, pore space fractions f_1 and f_2 and major semi-axes a_1 and a_2. The pore aspect ratios can be determined from thin section image analysis, and in this work they are fixed, for all well samples, as α_1 = 0.05 and α_2 = 0.55. These values consider the results found by Lima Neto (2015), being representative for micro and macro-meso pores, respectively.

The pore fractions f_1 and f_2 are determined for each well sample using the DEM model, as shown in Fig. 14. From this figure, it is possible to see a considerable scatter on the relation between log measured compressional velocity Vp and MLR porosity. This spreading can be associated to the occurrence of different pore types, since the pore type 1 is characterized by a more compressive pore shape, giving to

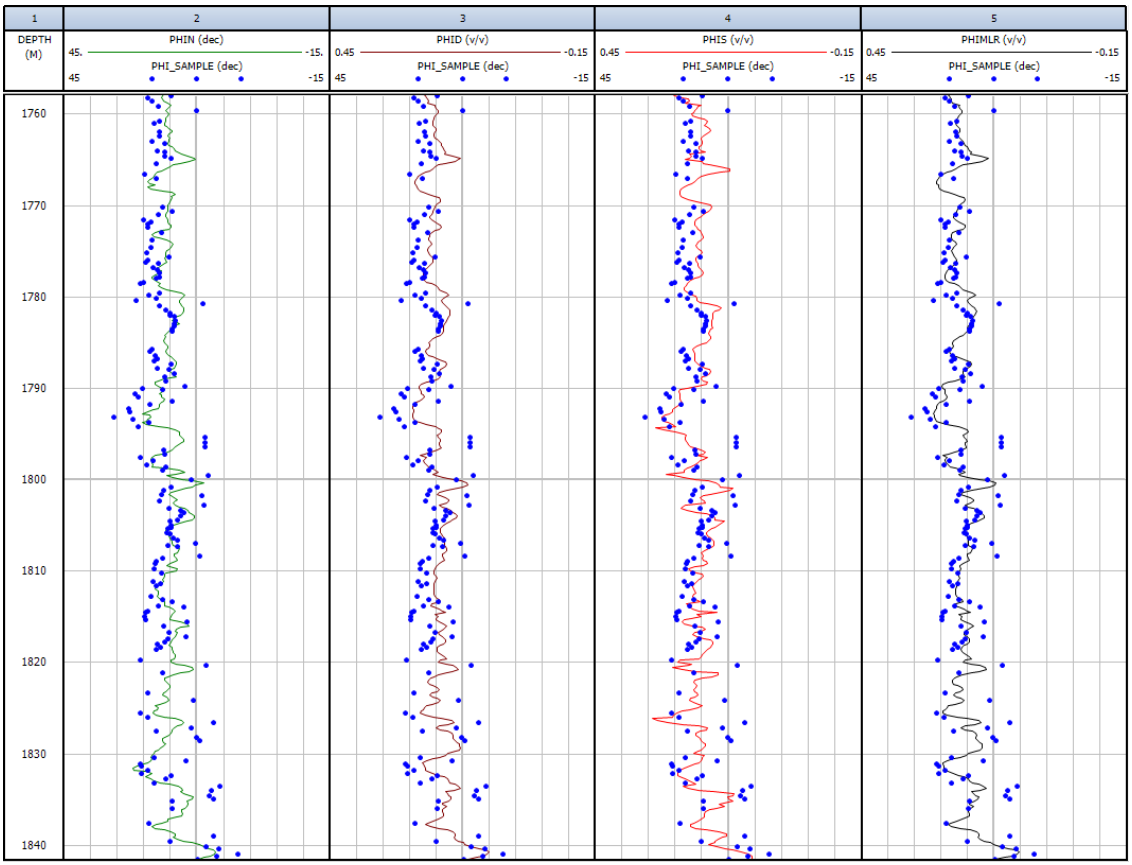

Figure 13: Log plot of porosity showing from the left to the right: 1 - the porosity measured from neutron log, 2 - the density porosity, 3 - the sonic porosity, and 4 - the porosity estimated by the Multiple Linear Regression (MLR) approach. The blue data points represent the measured porosity from core samples.

the samples lower velocity values, and the pore type 2 is characterized by a stiffer pore format, giving higher velocities than pore type 1.

To perform the estimation of f_1 and f_2, dry ellipsoidal inclusions are initially considered in a nonporous host medium composed by the mineral calcite, with bulk and shear moduli, respectively given by 70.8 and 30.3 GPa. The dry inclusions are subsequently saturated with Gassmann (1951) equations considering the oil and water saturations and their respective bulk moduli, given by 1.69 and 2.94 GPa. Thus, the pore fractions f_1 and f_2 are estimated by modeling the DEM Vp with the smallest error when compared to the measured Vp.

The Fig. 15-8 shows the measured and DEM estimated compressional velocities. The result shows a good agreement between them, validating the pore type fraction prediction. Since DEM model allows the estimative of bulk and shear moduli of the rock (see Appendix B), the shear velocity Vs is estimated, which is also show in Fig. 15-8. The absence of the shear slowness log does not allow the validation of Vs prediction, but its estimative has a considerable applicability on seismic analysis of porous media.

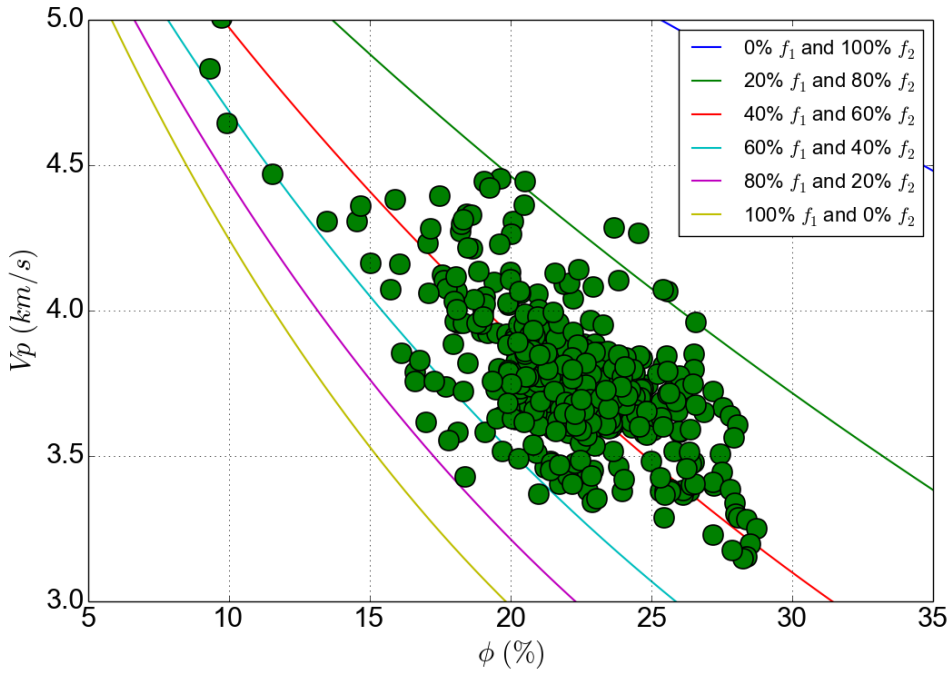

Figure 14: DEM rock physics template for Vp and porosity ϕ. The curves represent different pore fractions f_1 and f_2 for a dual porosity model with inclusion aspect ratios of α_1 = 0.05 and α_2 = 0.55 in a calcitic host medium. The data points relate the measured sonic velocity and the MLR porosity.

The estimated pore fractions f_1 and f_2 are shown in Fig. 15-9. The results indicate the predominant occurrence of pore type 2, although some intervals present relevant fractions of pore type 1, principally those containing lime mud fractions.

The pore size parameterization is improved by applying a Flow Unit (FU) classification following the graphical method of Gunter *et al.* (1997), which considers the storage and flow capacity of the core samples. This approach allowed identifying four flow units, as showed in Fig. 15-3, with the depth range presented in Table 1. According to the textural description in Fig. 15-2, the FU's 1 and 3 are composed by grainstones and packstones with some cemented intervals, while the FU's 2 and 4 comprises mainly formations with occurrence of lime mud, like mudstones and wackestones.

Table 1: The depth range and the major semi-axes a_1 and a_2 for each FU, used for specific surface prediction.

Flow Unit (FU)	Depth section (m)	a_1 (mm)	a_2 (mm)
1	1758.0 - 1789.1	0.10	0.50
2	1789.1 - 1803.6	0.01	0.06
3	1803.6 - 1818.6	0.20	0.50
4	1818.6 - 1841.5	0.01	0.05

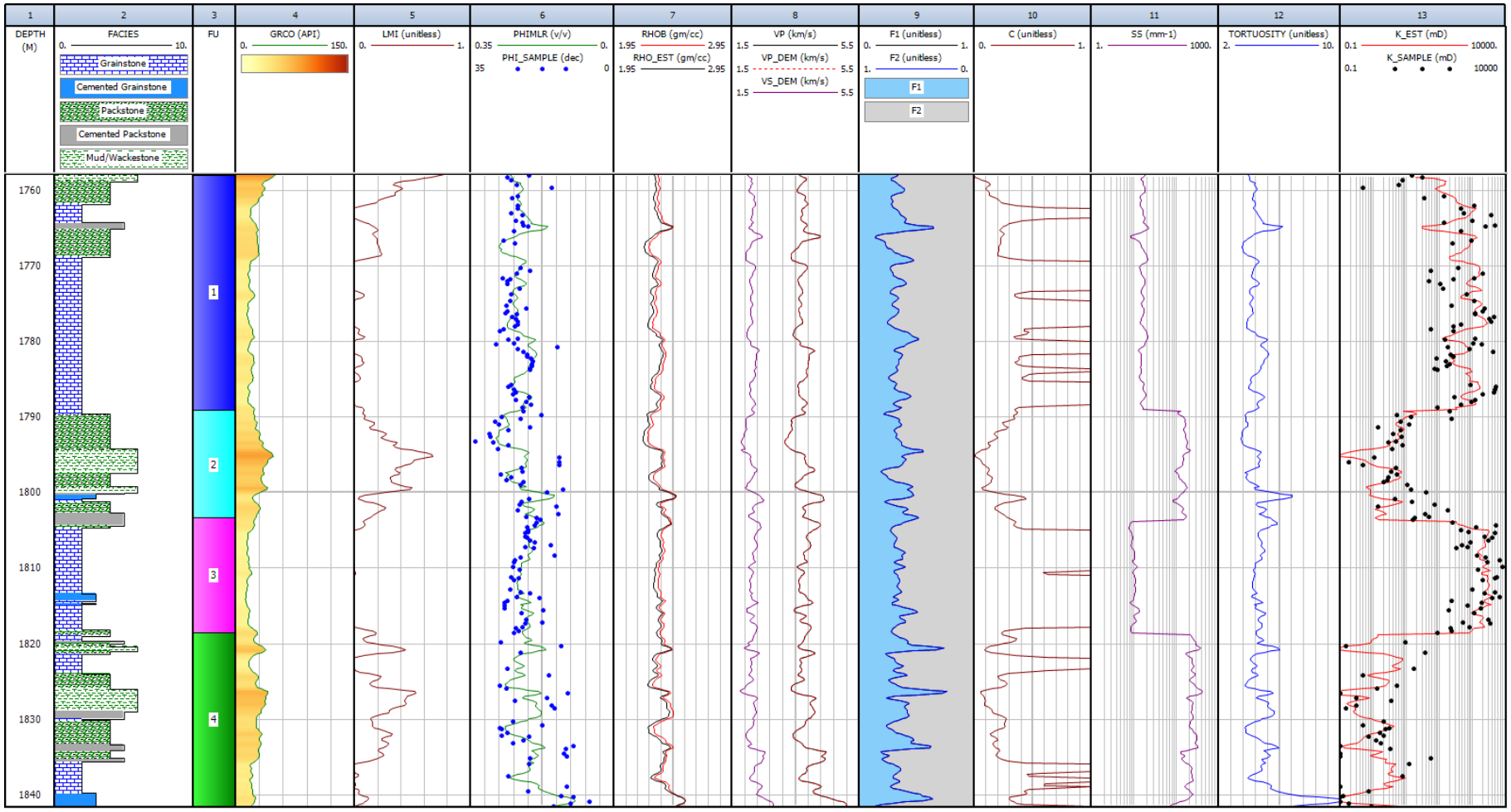

Figure 15: Log plot showing from the left to the right: 1 - depth, 2 - textural description, 3 - flow unit classification, 4 - gamma ray log, 5 - lime mud index, 6 - core sample and MLR porosities, 7 - log measured and estimated bulk densities, 8 - log measured Vp and Vp and Vs derived from DEM model, 9 - pore fractions estimated through the DEM model, 10 - pore connectivity, 11 - specific surface, 12 - tortuosity, and 13 - core sample and estimated permeabilities.

The semi-axes a_1 and a_2 are also shown in Table 1, being determined qualitatively from thin sections images, considering the textural interpretation for each FU and the Choquette and Pray (1970) pore size classification (micropores < 0.0625 mm; 0.0625 mm < mesopores < 4 mm; 4 mm < megapores < 256 mm). The pore size a_1 defines smaller and more compressive pores in the rock framework, while pore size a_2 represents larger and stiffer pores. According to the Choquette and Pray classification, the FU's 1 and 3 are composed mainly for pore sizes in the mesopore scale, while the FU's 2 and 4 by pores in the micropore scale, with a_2 close to the limit between micro and mesopores. This result reflects the geological interpretation for each interval.

The result for the specific surface S is presented in Fig. 15-11, with the FU's 2 and 4 showing the highest values among all intervals, indicating a more complex pore geometry. In contrast, the FU's 1 and 3 show small S estimative, which reflect a good sort and arrangement of grains. These observations correlate well with the corresponding interval flow and storage capacity.

The connectivity function c (Fig. 15-10) is computed considering the effect of carbonatic mud on the pore connectivity through the lime mud volume χ (Fig. 15-5), which was computed from gamma ray γ log (Fig. 15-4), using the conventional approach given by Eq. 2.4, considering the thresholds γ_{clean} = 20 API for clean carbonate, and γ_{mud} = 60 API for lime mud. The other parameters χ_{th}, χ_c and d for the connectivity function c are defined as 0, 0.7 and 0.2, respectively.

The tortuosity prediction (Fig. 15-12) considers the MLR porosity (Fig. 15-6) and a fixed cementation coefficient m = 2.0 for all well samples. The estimated tortuosity ranges from 3.5 to 10.7, and the higher values are found in the FU 4, which represents the more cemented interval. Note also in Fig. 15-7, the good agreement between log measured and predicted bulk density, which was derived from the well-know mass balance equation, considering the water and oil saturations. Its estimative was employed during the DEM model procedure.

After estimating all parameters of the modified Kozeny-Carman model, the permeability was calculated through Eq. 2.1, with the results shown in Fig. 15-13, where the data points represent the core permeability. As observed, the permeability estimated by the new method shows reasonable correlation with the measured values in all intervals. Although most well samples have good porosity values and small tortuosity variations, the FU's 1 and 3, that have the highest permeability values, have good pore connectivity and small specific surface values, while the FU's 2 and 4 have a poor pore connectivity and higher specific surface values, which consequently provides low

permeability values.

The Fig. 16 shows a crossplot comparing the log of estimated and measured permeability from core samples, where the data points are colored according to the Flow Unit classification. The correlation coefficient between the log of measured and predicted permeability is R^2 = 0.76. The good agreement validates the applicability of the proposed methodology, which takes into account the pore geometry modeling and the pore connectivity.

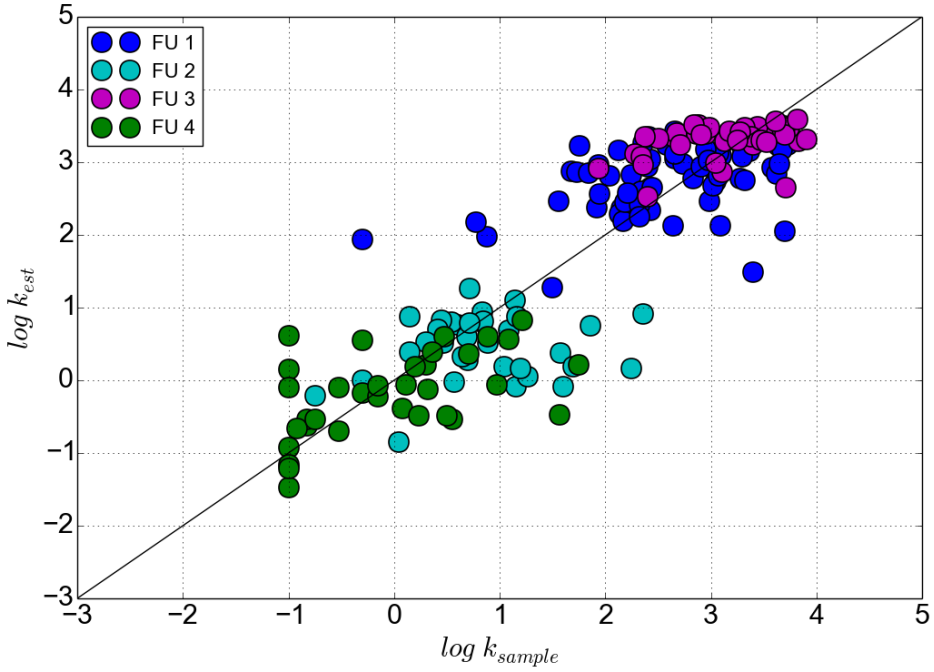

Figure 16: Comparison between the log of estimated permeability k_{est} and the log of measured permeability from core samples k_{sample}. The data points are colored according to the Flow Unit (FU) classification.

5 Discussion

The first question that can be arrised in the method is: which are the advantages of considering the pore geometry and connectivity during permeability modeling? We have seen from previous works and from the dataset in Fig. 12 that single relations between permeability and porosity are not able to provide reliable predictions of permeability. This lack of correspondence indicates that other pore related parameters, involving shape, size and connectivity, appear to control the flow capacity of the rocks, and the physical models that take into account these effects are a promise to improve substantially the permeability estimation.

In this sense, the method has an advantage in considering the effects of specific surface, flow path tortuosity and pore connectivity on permeability prediction, which proved its applicability in an Albian carbonate reservoir through a correlation coefficient R^2 = 0.76 between measured and estimated permeability. The error associated to this estimative is originated from many factors, including the physical model assumptions, which initially considers a pipe-like geometry, and the uncertainties associated to the model parameter estimations.

The first of all, and perhaps the least important, is the uncertainty related to the porosity prediction, which involves the model assumptions and the uncertainties of pore fluid and mineralogical content during the estimative of neutron, density and sonic porosity. According to the sensitivity analysis, these errors provide a small influence on permeability when compared to the effects of pore geometric parameters.

Since the specific surface approach has an advantage in considering the effect of N pore types, the permeability was estimated by modeling a dual porosity rock framework containing a more compressive pore with α_1 = 0.05 and a stiffer pore format with α_2 = 0.55, which are commonly attributed to micro and macro-meso pores, respectively. The fractions of these pore types were estimated through the DEM model, considering their effect on the spreading between Vp and porosity ϕ, as shown in Fig. 14. The velocities have been employed on permeability prediction in works of Fabricius *et al.* (2007) and Saxena (2017), and in this study, the pore geometry seems to be a bridge

to correlate the elastic behavior with the flow capacity of rocks.

About the pore size parameterization, the Flow Unit classification performed the reservoir zoning by applying the graphical method of Gunter *et al.* (1997). This approach was chosen because the laboratory core data covers the entire reservoir, and it returns stratigraphically continuous intervals, however any facies classification derived from well logs can be used to perform the reservoir zoning. The pore sizes a_1 and a_2 were fixed for each FU according to the geological interpretation following the Choquette and Pray (1970) classification, although they do not provide an accurate description of pore geometry variations throughout the studied interval.

The fixed pore shape formats, characterized by the aspect ratios α_1 and α_2, are not necessarily correlated with the pore sizes a_1 and a_2, even though some researchers have associated them with micro and macro-meso pores, respectively. According the results, the UF's 1 and 3 presented both pore types at mesopore scale, while UF's 2 and 4 presented pore types at micropore scale, with a_2 close to the limit between micro and mesopores. This assumption assumes that different pore shapes can occur at any pore size scale, being able to substantially modify the flow capacity of the rocks.

The Kozeny-Carman model was modified through a connectivity function based on percolation theory to model the effect of pore connectivity. The connectivity equation assumes that the amount of carbonatic mud controls the flow capacity of the rock, since it partially fills the porous space between the carbonatic grains, reducing the pore throat size. The lime mud fraction was derived from the gamma ray log, which presents a strong correlation with the permeability data obtained in laboratory tests. During this estimative, the presence of lime mud was associated to high radioactivity values, since the elements Potassium, Thorium and Uranium are related to the clay and organic matter contents, commonly deposited in low energy environments.

The tortuosity was estimated by a conventional approach based on porosity and Archie's cementation coefficient m, which takes into account the concept of electrical tortuosity. Since this simplified model fixes m = 2 for all well samples, the results show small variations in the UF's 1, 2 and 3, with UF 4 presenting the higher tortuosity values. This increasing is associated to the porosity reduction by diagenetic processes, involving cementation and dolomitization, which show a clear relation with the oil migration, since the cementation is more expressive in the water zone.

Finally, since the permeability model takes into account these volumetric and geometric parameters, it is possible to analyze, from Fig. 15, how permeability is influenced for each one. For it, two core samples with similar porosity and different permeability

values were analyzed. The core sample 1, localized at depth 1771.0 m, has measured porosity and permeability equal to 23.7% and 2000.0 mD, respectively, while the core sample 2, localized at 1832.8 m, presents laboratory porosity and permeability equal to 22.0% and 1.2 mD, respectively. The estimated values from MLR porosity and modified KC model are respectively 23.8% and 1630.5 mD for sample 1, and 20.8% and 0.4 mD for sample 2, having good correlation with the measured values.

The sample 1 is a grainstone localized at FU 1, and the high permeability value can be associated to a better size, sorting and arrangement of the grains and the absence of lime mud, giving to the rock high pore connectivity. About the estimated pore geometric parameters, the sample has 70.7% of the modeled pore space composed by more rounded pores and the pore sizes in the mesopore scale, which give to the sample a small specific surface value. Considering the low tortuosity value, the sample has all necessary characteristics for a good flow capacity, which is confirmed with the high laboratory permeability value.

In contrast, the sample 2, localized at FU 4, has a very small permeability value, although it has a considerable storage capacity. This fact can be explained by the high volume of lime mud, which reduces the pore connectivity to 19.7%. About the pore geometric parameters, the sample has 47.4% of the modeled pore space composed by more compressive pores and the pore sizes in the micropore scale, which return a high specific surface value. The tortuosity has also a small value, close to 5, and these estimative justify the low permeability value for a rock with 22.0% of porosity.

6 Conclusions

This work proposed a new approach to account the effect of pore geometry and pore connectivity on permeability prediction through a modified Kozeny-Carman model. From the studied Albian carbonate dataset, the results showed that the lime mud volume and the presence of more compressive and smaller pores make the pore geometry complex, reducing the permeability of rocks, even for high porosities.

The results show that the proposed method can reproduce reasonably well permeability measurements over the range of 0.1 to 8100 mD in oil and oil-water transition zones comprising different carbonate textures, with porosity varying from 6 to 34%. It confirms that pore geometry and pore connectivity are the main parameters that control the fluid flow, which can be used in specialized models to reduce the permeability estimation errors.

Finally, since the modified KC model produces continuous permeability estimative along the well from basic geophysical logs, the approach reduces the dependence of special logs, e.g., NMR, and the necessity for large number of core sample measurements. These advantages increase the model applicability for older well datasets, and can reduce the costs involving the special log acquisition and core sample extraction.

6.1 Suggestions for Future Research

- To study the model applicability in a laboratory dataset with the pore geometric parameters obtained from digital image analysis, aiming to improve the parameterization of porosity, specific surface and tortuosity, principally in pre-salt reservoirs;
- To derive a connectivity function based on coordination number or other geometric parameter using the percolation theory, in a similar approach develop by Bernabé *et al.* (2010). This modification will allow estimate pore connectivity from computational methods in laboratory;

- Improvement of the computational performance of the DEM inclusion model, and apply other models to characterize the rock framework, like T-matrix and Hudson (1980) model, which takes into account the anisotropic effects;
- Improve the tortuosity estimative from methods that consider the pore geometry and percolation theory, like Ghanbarian *et al.* (2013).

References

ARCHIE, G. E. The electrical resistivity log as an aid in determining some reservoir characteristics. *Transactions of the American Institute of Mining and Metallurgical Engineers*, v. 146, p. 54–62, 1942.

AVSETH, P.; MUKERJI, T.; MAVKO, G. *Quantitative Seismic Interpretation: Applying Rock Physics Tools to Reduce Interpretation Risk*. [S.l.]: Cambridge University Press, 2005. ISBN 9780521816014.

BATZLE, M.; WANG, Z. Seismic properties of pore fluids. *Geophysics*, v. 57, n. 11, p. 1396–1408, 1992.

BERNABÉ, Y.; LI, M.; MAINEULT, A. Permeability and pore connectivity: A new model based on network simulations. *Journal of Geophysical Research: Solid Earth*, v. 115, n. B10203, 2010.

BERNABÉ, Y.; ZAMORA, M.; LI, M.; MAINEULT, A.; TANG, Y. B. Pore connectivity, permeability, and electrical formation factor: A new model and comparison to experimental data. *Journal of Geophysical Research: Solid Earth*, v. 116, n. B11204, 2011.

BERRYMAN, J. G. Single-scattering approximations for coefficients in biot's equations of poroelasticity. *Acoustical Society of America Journal*, v. 91, p. 551–571, 1992.

CARMAN, P. *L'écoulement des gaz à travers les milieux poreux*. [S.l.]: Institut National des Sciences et Techniques Nucléaires, 1961. (Bibiothèque des sciences et techniques nucléaires).

CARRASQUILLA, A.; NELSON, P. F. F. Petrophysical evaluation of a carbonate reservoir in campos basin - southeastern brazil. In: *84th Annual International Meeting, Expanded Abstracts*. Denver, Colorado: Society of Exploration Geophysicists, 2014. p. 2714–2718.

CHOQUETTE, P. W.; PRAY, L. C. Geologic nomenclature and classification of porosity in sedimentary carbonates. *AAPG Bulletin*, American Association of Petroleum Geologists (AAPG), v. 54, p. 207–250, 1970.

COATES, G. R.; DUMANOIR, J. L. New approach to improved log-derived permeability. In: *SPWLA 14th Annual Logging Symposium*. Lafayette, Louisiana: Society of Petrophysicists and Well-Log Analysts, 1973. v. 15, p. 17–31.

DUNHAM, R. J. Classification of carbonate rocks according to depositional texture. In: HAM, W. E. (Ed.). *Classification of Carbonate Rocks, A Symposium*. Tulsa: American Association of Petroleum Geologists, 1962. p. 108–121.

EBERLI, G. P.; BAECHLE, G. T.; ANSELMETTI, F. S.; INCZE, M. L. Factors controlling elastic properties in carbonate sediments and rocks. *The Leading Edge*, v. 22, n. 7, p. 654–660, 2003.

FABRICIUS, I. L.; BAECHLE, G.; EBERLI, G. P.; WEGER, R. Estimating permeability of carbonate rocks from porosity and vp/vs. *Geophysics*, v. 72, n. 5, p. E185–E191, 2007.

GASSMANN, F. Über die elastizität poröser medien. *Verteljahrsschrist der Naturforschenden Gesellschaft*, v. 96, p. 1–23, 1951.

GHANBARIAN, B.; HUNT, A.; SAHIMI, M.; EWING, R. P.; SKINNER, T. Percolation theory generates a physically based description of tortuosity in saturated and unsaturated porous media. *Soil Science Society of America Journal*, v. 77, p. 1920, 11 2013.

GUNTER, G. W.; FINNERAN, J. M.; HARTMANN, D. J.; MILLER, J. D. Early determination of reservoir flow units using an integrated petrophysical method. In: *SPE Annual Technical Conference and Exhibition*. San Antonio, Texas: Society of Petroleum Engineers, 1997. p. 373–380.

HEARST, J.; NELSON, P. *Well logging for physical properties*. [S.l.]: McGraw-Hill, 1985. ISBN 9780070276987.

HUANG, Z.; SHIMELD, J.; WILLIAMSON, M.; KATSUBE, J. Permeability prediction with artificial neural network modeling in the venture gas field, offshore eastern canada. *Geophysics*, v. 61, n. 2, p. 422–436, 1996.

HUDSON, J. A. Overall properties of a cracked solid. *Mathematical Proceedings of the Cambridge Philosophical Society*, Cambridge University Press, v. 88, n. 2, p. 371–384, 1980.

KATZ, A. J.; THOMPSON, A. H. Quantitative prediction of permeability in porous rock. *Physical Review B*, v. 34, n. 11, p. 8179–8181, 1986.

KUSTER, G. T.; TOKSÖZ, M. N. Velocity and attenuation of seismic waves in two-phase media. *Geophysics*, v. 39, p. 587–618, 1974.

LIMA, O. A. L. Water saturation and permeability from resistivity, dielectric, and porosity logs. *Geophysics*, v. 60, n. 6, p. 1756–1764, 1995.

LØNØY, A. Making sense of carbonate pore systems. *AAPG Bulletin*, v. 90, n. 9, p. 1381–1405, 2006.

MAVKO, G.; MUKERJI, T.; DVORKIN, J. *The Rock Physics Handbook: Tools for Seismic Analysis of Porous Media*. [S.l.]: Cambridge University Press, 2009. ISBN 9781139478328.

MAVKO, G.; NUR, A. The effect of a percolation threshold in the kozeny-carman relation. *Geophysics*, v. 62, n. 5, p. 1480–1482, 1997.

NELSON, P. H. Permeability-porosity relationships in sedimentary rocks. *Log Analyst*, v. 35, p. 38–62, 05 1994.

NETO, I. A. L. *Carbonate pore system evaluation under texture under control for prediction of microporosity aspect ratio and shear wave velocity, using the velocity-porosity-pressure relationship*. Tese (Thesis) — Universidade Estadual do Norte Fluminense, 2015.

PRASAD, M. Velocity-permeability relations within hydraulic units. *Geophysics*, v. 68, n. 1, p. 108–117, 2003.

SAXENA, V. Interacting-pore effective medium scheme for velocity inversion and permeability prediction. In: *SEG Technical Program Expanded Abstracts 2017*. Houston, TX: Society of Exploration Geophysicists, 2017. p. 3826–3830.

SCHÖN, J. *Physical Properties of Rocks: A Workbook*. [S.l.]: Elsevier, 2011. ISBN 9780444537966.

TIMUR, A. An investigation of permeability, porosity and residual water saturation relationships for sandstone reservoirs. *The Log Analyst*, v. 9, n. 4, p. 8–17, 1968.

WYLLIE, M. R. J.; GREGORY, A. R.; GARDNER, L. W. Elastic wave velocities in heterogeneous and porous media. *Geophysics*, v. 21, p. 41–70, 1956.

WYLLIE, M. R. J.; ROSE, W. D. Some theoretical considerations related to the quantitative evaluation of the physical characteristics of reservoir rock from electrical log data. *Journal of Petroleum Technology*, v. 2, n. 4, p. 105–118, 1950.

XU, S.; PAYNE, M. A. Modeling elastic properties in carbonate rocks. *The Leading Edge*, v. 28, p. 66–74, 2009.

APPENDIX A – The Kozeny-Carman Model

The Kozeny-Carman (KC) model (CARMAN, 1961) is a physical model that allows estimating the permeability of a porous medium through parameters such as porosity, specific surface, tortuosity and grain size. The derivation of the model is based on flow through a set of n tubes having a circular cross-section with radius R (Fig. 17).

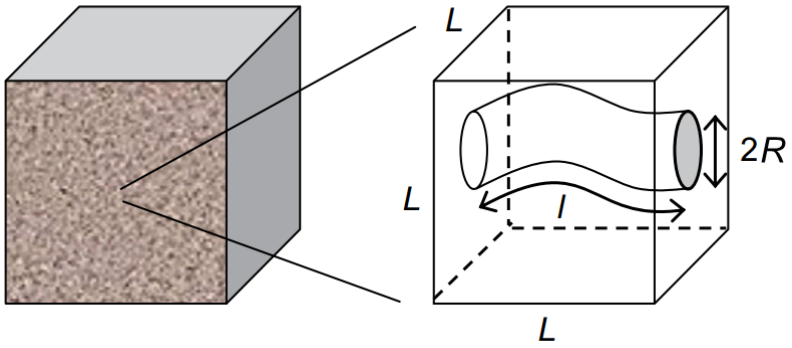

Figure 17: The KC model concept for a single tube with length l and radius R. The parameter L represents the length of the sample [Modified from Schön (2011)].

Thus, the flow for a given set of n tubes of radius R and length l can be described, according to Poiseulle's law, as

$$q = -\frac{n\pi R^4}{8\eta}\frac{\Delta P}{l}, \tag{A.1}$$

where q represents the flowing fluid volume per time, ΔP the pressure drop along the tubes and η the dynamic viscosity of the fluid.

The comparison with Darcy's law expressed by

$$q = -k\frac{A}{\eta}\frac{\Delta P}{L}, \tag{A.2}$$

where k is the permeability, L the length of the sample and A the cross-sectional area

of flow, gives the effective permeability of a porous medium expressed as

$$k = \frac{n\pi R^4 L}{8Al}. \tag{A.3}$$

Considering the concept of tortuosity, defined as the ratio of total flow-path length to length of the sample ($\tau = l/L$), the Eq. A.3 can be rewritten as

$$k = \frac{n\pi R^4}{8A\tau}. \tag{A.4}$$

Since the porosity ϕ for the pipe system described above is given by

$$\phi = \frac{n\pi R^2 l}{AL} = \frac{n\pi R^2 \tau}{A}, \tag{A.5}$$

and the specific surface S, defined as the ratio of porous surface area to rock bulk volume, is expressed as

$$S = \frac{2n\pi Rl}{AL} = \frac{2n\pi R\tau}{A} = \frac{2}{R}\frac{n\pi R^2\tau}{A} = \frac{2\phi}{R}, \tag{A.6}$$

the comparison of porosity equation (Eq. A.5) with the Eq. A.4 gives

$$k = \frac{\phi R^2}{8\tau^2}, \tag{A.7}$$

and finally, the correlation of specific surface equation (Eq. A.6) with Eq. A.7 gives

$$k = \frac{1}{2}\frac{\phi^3}{S^2\tau^2}, \tag{A.8}$$

which is known as the Kozeny-Carman equation, and as it can be observed, the permeability estimation depends only on porosity, specific surface and tortuosity.

From the analysis of Eq. A.8, the permeability has units of area (m^2), which defines it as a geometric measure. In the oil industry, the most commonly used unit is Darcy (D) or miliDarcy (mD), and the relation between these units is given by

$$1D = 0.9869\,10^{-12} m^2 \approx 1\mu m^2. \tag{A.9}$$

A common extension of the KC model is to consider a packing of identical spheres of diameter D. Although this granular pore space geometry is not consistent with

the pipe-like geometry, it is common to use the original KC functional form. Thus, considering a set of spheres, the specific surface S can be expressed in terms of porosity, through the equation

$$S = \frac{6(1-\phi)}{D}, \tag{A.10}$$

which leads to the permeability expression

$$k = \frac{1}{72}\frac{\phi^3}{(1-\phi)^2\tau^2}D^2. \tag{A.11}$$

There is also a diversity of models and relations derived from the KC equation.

APPENDIX B – The Differential Effective Medium Model

The Differential Effective Medium (DEM) model (BERRYMAN, 1992; MAVKO *et al.*, 2009) describes a composite material with two phases in which the elastic moduli changes due to infinitesimal additions of inclusions (phase 2) in a host medium (phase 1). This iterative process is continued until the desired proportion of the constituents is reached. In this theory, the formulation is given by a coupled system of ordinary differential equations derived from Kuster and Toksöz (1974) model to calculate bulk $K^*(\phi)$ and shear $\mu^*(\phi)$ moduli of the composite, as given by

$$(1-\phi)\frac{d}{d\phi}[K^*(\phi)] = (K_2 - K^*)P^{*2}(\phi), \tag{B.1}$$

$$(1-\phi)\frac{d}{d\phi}[\mu^*(\phi)] = (\mu_2 - \mu^*)Q^{*2}(\phi), \tag{B.2}$$

with initial conditions $K^*(0) = K_1$ and $\mu^*(0) = \mu_1$, where K_1 and μ_1 are, respectively, the bulk and shear moduli for the phase 1, K_2 and μ_2 are the bulk and shear moduli of inclusion phase 2, and P^{*2} and Q^{*2} are geometrical factors depending on the aspect ratio α of the inclusions, and their superscript $*2$ indicates that these factors are for an inclusion of material 2 in a background medium with effective moduli K^* and μ^*. For a porous medium, ϕ is the porosity and $d\phi$ is the infinitesimal increment in porosity.

The DEM model does not treat each constituent symmetrically, and for multiple inclusion shapes, the effective moduli depend not only on the final volume concentrations of the constituents but also on the order in which the incremental additions are made. Because the inclusions are isolated with respect to flow, this approach simulates high-frequency saturated rock behavior, and at low frequencies it is better to estimate the effective moduli for dry inclusions and then saturate them with the Gassmann (1951) equations (MAVKO *et al.*, 2009).

APPENDIX C – The Specific Surface Approach

The specific surface approach considers the pores like ellipsoidal inclusions with semi-axes a and b (Fig. 2), aspect ratio α and eccentricity e, respectively given by b/a and $\sqrt{1-\alpha^2}$, and surface area A_{ellip} and volume V_{ellip} defined by

$$A_{ellip} = 2\pi a^2 \left(1 + \frac{1-e^2}{e} arctanh(e)\right), \tag{C.1}$$

$$V_{ellip} = \frac{4\pi}{3} a^3 \alpha. \tag{C.2}$$

Considering a porous space composed by N pore types, where for each pore type the inclusions have the same shape and size, the total pore surface area A_{pore} and total pore volume V_{pore} can be expressed by

$$A_{pore} = \sum_{i=1}^{N} M_i A_{ellip\,i}, \tag{C.3}$$

$$V_{pore} = \sum_{i=1}^{N} M_i V_{ellip\,i}, \tag{C.4}$$

where M_i represents the number of inclusions for each pore type.

The specific surface with respect to pore volume S_{pore} can then be expressed as

$$S_{pore} = \frac{A_{pore}}{V_{pore}} = \frac{\sum_{i=1}^{N} M_i A_{ellip\,i}}{\sum_{i=1}^{N} M_i V_{ellip\,i}}. \tag{C.5}$$

Considering the porosity ϕ as the ratio of total pore volume V_{pore} to the bulk volume of the rock V_{bulk}, it can be represented as a sum of the volume fractions x_i of the N

pore types, as given by

$$\phi = \frac{V_{pore}}{V_{bulk}} = \sum_{i=1}^{N} x_i, \tag{C.6}$$

where the volume fraction x_i can be correlated with the pore space fraction f_i through the equation

$$x_i = f_i \phi. \tag{C.7}$$

Substituting the Eq. C.4 in Eq. C.6 gives

$$\frac{\sum_{i=1}^{N} M_i V_{ellip\,i}}{V_{bulk}} = \sum_{i=1}^{N} x_i, \tag{C.8}$$

and from this relation it is possible to state that

$$M_i V_{ellip\,i} = x_i V_{bulk}, \tag{C.9}$$

which allows to estimate the number of inclusions for each pore type M_i as

$$M_i = x_i \frac{V_{bulk}}{V_{ellip\,i}}. \tag{C.10}$$

Substituting the Eq. C.10 in Eq. C.5 gives

$$S_{pore} = \frac{\sum_{i=1}^{N} x_i \frac{A_{ellip\,i}}{V_{ellip\,i}}}{\sum_{i=1}^{N} x_i}, \tag{C.11}$$

in which, considering the Eq. C.6, is the same as

$$S_{pore} = \frac{\sum_{i=1}^{N} x_i \frac{A_{ellip\,i}}{V_{ellip\,i}}}{\phi}. \tag{C.12}$$

Since the specific surface with respect to the bulk volume is $S = S_{pore}\phi$, the specific surface can be expressed as

$$S = \sum_{i=1}^{N} x_i \frac{A_{ellip\,i}}{V_{ellip\,i}}. \tag{C.13}$$

As can be observed from Eq. C.1, C.2 and C.13, the specific surface S depends only on the concentration x (volumetric parameter), the aspect ratio α (pore shape) and the major semi-axis a (pore size) of the N inclusion types.

APPENDIX D – The Gassmann Model

One of the challenges of rock physics modeling is the understanding and prediction of how velocities and impedance depend on the porous fluid (AVSETH *et al.*, 2005). In this context, the fluid substitution models estimate the elastic properties of a porous rock at one fluid state, and predicts these properties for another fluid state (MAVKO *et al.*, 2009).

The Gassmann model assumes that the rock is macroscopically homogeneous and isotropic, and it is valid only at low frequencies, such that the induced pore pressures are equilibrated throughout the pore space. In other words, there is sufficient time for the pore fluid to flow and reduce the effect of the wave-induced pore pressure (SCHÖN, 2011; MAVKO *et al.*, 2009).

Considering the effects of rock deformation, the equation for calculating the bulk modulus of a saturated rock K_{sat} is expressed by

$$K_{sat} = K_{dry} + \frac{\left(1 - \frac{K_{dry}}{K_0}\right)^2}{\frac{\phi}{K_{fl}} + \frac{1-\phi}{K_0} - \frac{K_{dry}}{K_0^2}}, \tag{D.1}$$

and for dry rocks as

$$K_{dry} = \frac{K_{sat}\left(\frac{\phi K_0}{K_{fl}} + 1 - \phi\right) - K_0}{\frac{\phi K_0}{K_{fl}} + \frac{K_{sat}}{K_0} - 1 - \phi}, \tag{D.2}$$

where K_{dry} is the effective bulk modulus of the dry rock, K_0 the bulk modulus of the solid rock component, K_{fl} the bulk modulus of the pore fluid, and ϕ the porosity.

Because the shear modulus μ is independent of the pore fluid, it is the same for both saturated and dry rocks:

$$\mu_{sat} = \mu_{dry}. \tag{D.3}$$

The calculation of the density ρ can be performed using mass balance equation

$$\rho = \rho_0(1-\phi) + \rho_{fl}\phi, \tag{D.4}$$

where ρ_0 and ρ_{fl} represent the density of solid rock component and of the pore fluid, respectively, and ϕ the porosity of the rock.

Thus, considering the equations for elastic moduli K and μ and density ρ, the compressional velocity Vp and shear velocity Vs can be estimated from equations

$$Vp = \sqrt{\frac{K + \frac{4}{3}\mu}{\rho}}, \tag{D.5}$$

$$Vs = \sqrt{\frac{\mu}{\rho}}. \tag{D.6}$$

This sequential description allows predicting saturated-rock velocities from dry-rock velocities, and vice versa.

Index